Crystal anisotropy and spin-polarized photoluminescence of ordered $Ga_xIn_{1-x}P$

B. Fluegel, Y. Zhang, A. Mascarenhas, J. F. Geisz, J. M. Olson, and A. Duda
National Renewable Energy Laboratory, Golden, Colorado 80401
(Received 6 July 1999)

Two-color up-conversion time-resolved photoluminescence and time-resolved absorption are used to study spin relaxation of near-resonant heavy-hole excitons in spontaneously ordered $Ga_xIn_{1-x}P$. The photoluminescence anisotropy is studied as a function of crystal direction, revealing a strong dependence on the light orientation with respect to the ordering axis. The maximum observed polarization is 0.8, and indicates that the polarization is near unity shortly after excitation. The carrier spin-relaxation time is 150 ps.
[S0163-1829(99)50940-5]

Spin-polarized photoluminescence is a valuable method for identifying optical transitions in semiconductors. By exciting with circularly polarized light, and analyzing the degree of circular polarization in the photoluminescence (PL), heavy-hole (HH), and light-hole (LH) transitions can be distinguished in quantum well structures.[1] The technique is sensitive to crystal symmetry and the k vectors of the exciting and luminescing fields. In zinc-blende multiple quantum wells (MQW), selective optical pumping of one angular momentum state is possible because of valence-band splitting (VBS) of HH and LH bands. This results from the [001]-oriented barriers reducing the cubic $\bar{4}3m$ point-group symmetry to tetragonal $\bar{4}2m$. A similar splitting exists in spontaneously ordered $Ga_xIn_{1-x}P$ where special growth conditions cause the alloyed cations to approximate a monolayer superlattice of alternating In-rich and Ga-rich planes.[2] Because the planes are in the $\langle 111\rangle$ direction, the $\bar{4}3m$ symmetry is reduced to $3m$, resulting in a VBS of HH and LH bands.

Spin-polarized PL has been observed in ordered $Ga_xIn_{1-x}P$ (Ref. 3) from near-resonant pumping of the HH exciton, but only along the growth direction. In contrast to [001] MQW's, these CuPt-ordered alloys have an ordering direction along $\langle 111\rangle_B$, which is 55° from the nominal growth direction. Spectroscopy measurements in these epilayer samples have been hindered by the fact that this tilted ordering axis determines the optical axis and the angular-momentum quantization direction.

This complication has been overcome with microspectroscopy techniques that access high-symmetry directions.[4–6] Here, we combine these techniques with up-conversion time-resolved photoluminescence to measure 4 K spin-relaxation times and polarization both parallel to, and at angles to the ordering direction.

The $Ga_xIn_{1-x}P$ sample was grown to a thickness of 10 μm by atmospheric-pressure organometallic vapor phase epitaxy on a (001) GaAs substrate cut 6° toward $\langle 111\rangle_B$. The measured gallium fraction, x, was within $|\delta x| = 5\times10^{-3}$ of the low-temperature lattice-matched value, 0.52. The low-temperature photoluminescence excitation spectrum shows a Stokes shift of 4 meV, and a VBS of 23 meV, which corresponds[7] to an ordering parameter of 0.46. Along with the growth face, two special surfaces were prepared by (1) cleaving along $(\bar{1}\bar{1}0)$ to allow light propagation perpendicular to ordering, and (2) polishing a $(1\bar{1}\bar{1})$ face to allow light propagation parallel to the ordering axis. These faces are illustrated in Fig. 1.

The experimental apparatus is a two-color up-conversion time-resolved photoluminescence measurement.[8] 150 fs pulses from an amplified Ti:sapphire laser were used to pump both an optical parametric amplifier (OPA), and the up-conversion. The OPA produced 60-fs tunable pulses centered at the HH exciton absorption energy. These pulses were spectrally narrowed in a grating pulse shaper[9] resulting in a temporal width of 1.3 ps, and focussed onto the sample with conventional optics. The energy density was 3 μJ/cm^2. A liquid crystal variable retarder allowed computer control of the circular polarization without any moving optics. PL was collected in near back-reflection, analyzed with a broadband waveplate, then sent to a spectrometer and multichannel detector for time-integrated detection, and to a sum-frequency-generation crystal for time-resolved detection. A 0.5-mm $LiIO_3$ crystal mixed the PL with the amplified Ti: sapphire pulse that had been filtered to a 3 nm bandwidth around 806 nm. Up-converted light was detected with a photon-counting microchannel plate photomultiplier tube. Parallel circular (σ^- pump, σ^- PL) and orthogonal circular (σ^+ pump, σ^- PL) photoluminescence, $I_\parallel$ and $I_\perp$, were collected. Reciprocal results could be obtained by rotating the analyzer by 90°.

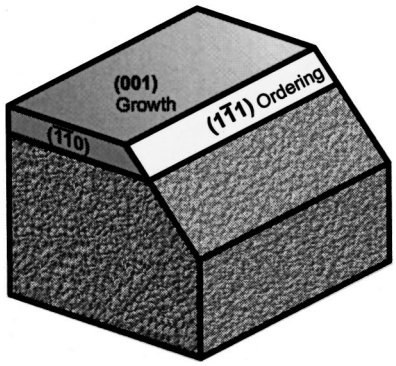

FIG. 1. Diagram of ordered $Ga_xIn_{1-x}P$ epilayer on GaAs substrate, showing the three measurement directions. The 6° tilt of the substrate is not shown, and the actual growth direction is [001] tilted 6° toward $[1\bar{1}\bar{1}]$.

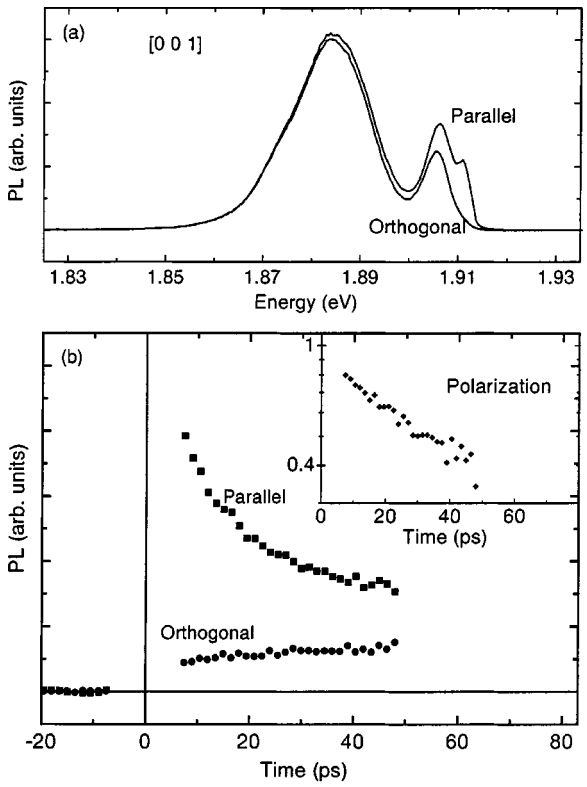

FIG. 2. PL in the [001] (growth) direction. (a): Spectrally resolved time-integrated PL polarized parallel to and orthogonal to the circularly polarized pump. (b): Time-resolved PL at the peak of the HH, under identical excitation conditions. Inset: log plot of degree of polarization computed from the parallel and orthogonal components.

Figure 2(a) shows time-integrated PL from excitation normal to the growth face. The PL consists of a low-energy peak,[3,10] which we will not discuss, and an excitonic peak at higher energy. The excitation wavelength can be identified from the scattered light at slightly higher energy. This strong pump scatter results from a surface morphology that is characteristic of thick samples. Similar effects arise from using the beveled $(1\bar{1}1)$ face, and the very narrow $(\bar{1}10)$ face. Limitations caused by this scatter are minimized by careful attention to the laser temporal and spectral width. The pulse shaper is used to obtain very sharp attenuation outside the passband, which is smaller than the Stokes shift of the sample. In the time-resolved measurement, data near $t=0$ has been gated out to eliminate all contributions from scatter. Spectral overlap with the low-energy PL does not contribute to the time-resolved data since the low-energy PL is spread over $\approx$50 ns.

The static polarization, $\rho \equiv (I_{\parallel}-I_{\perp})/(I_{\parallel}+I_{\perp})$, at the exciton PL energy in Fig. 2(a) is 0.20. In general, an incomplete static polarization may result either from a large rate of spin decay, $1/\tau_s$, or a smaller rate of population decay, $1/\tau_r$. For the case of exponential decays, these predict a static polarization of[11]

$$\rho = \frac{\tau_s}{\tau_s + \tau_r}. \tag{1}$$

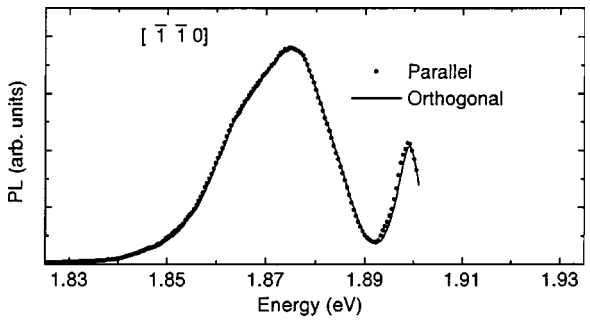

FIG. 3. Time-integrated PL in the $[\bar{1}10]$ direction, i.e., propagating the light orthogonal to the ordering axis.

These two contributions can be separated in the time-resolved data of Fig. 2(b), which plots time traces of the parallel circular, orthogonal circular, and $\rho(t)$. At the earliest observable times, the orthogonal polarization is clearly seen to be rising, in contrast to Ref. 3. The initial polarization is therefore higher than the time-integrated result and decays faster than the population. In the simple rate equations of Ref. 12, $\rho(t)$ decays as $\exp(-2t/\tau_s)$ and the total parallel+orthogonal intensity, $\equiv I_{\rm tot}$, decays as $\exp(-t/\tau_r)$. The total PL of Fig 2, (not plotted) is strongly nonexponential, indicating a density-dependent decay, or a decay channel that saturates. Direct detection using a picosecond detector measured a long-time component to $I_{\rm tot}$ of 400 ps. In the case of the polarization decay, $\rho(t)$, the population is normalized out, giving an exponential decay of $\tau_s = 150$ ps.

Even in the absence of spin and population decay, the polarization at $t=0$ may still be <1 because of the orientation of the light wave vectors with respect to the ordering direction. The measurements of Fig. 2 and Ref. 3 use the easily accessed growth direction, which differs from the ordering axis. Such a measurement, in general, will not create a pure spin population of carriers, and each spin population will not couple solely to one light polarization. Figure 3 shows the special case where PL is measured from the $[\bar{1}10]$ direction. This is perpendicular to the ordering direction, resulting in very little circular polarization of the PL. In contrast, by orienting the light along $[1\bar{1}1]$, i.e., parallel to ordering, the much stronger polarization of Fig. 4 is achieved. Here, the static polarization is 0.28, and the time-resolved PL shows a polarization that extrapolates to nearly unity at $t=0$.

To compare with these measured values; we have computed a maximum initial polarization by summing interband dipole matrix elements for HH and conduction-band (CB) states in a basis appropriate for the laser direction. The population generated is then used to sum up recombination rates for each PL polarization. For simplicity, the electron population is assumed to remain unrelaxed from its initially excited spin. The HH population is treated as either completely unrelaxed, or completely relaxed.[13] The results are shown in Table I. A relaxed hole population is a commonly used assumption in zinc-blende semiconductors because of a strong coupling between angular momentum and **k**. However, ordered $Ga_xIn_{1-x}P$ is similar to the situation in which a uniaxial stress is applied to a zinc-blende semiconductor. The $\mathbf{k}\cdot\hat{\mathbf{L}}$ coupling is negligible for states with $|\mathbf{k}|\approx 0$ as a

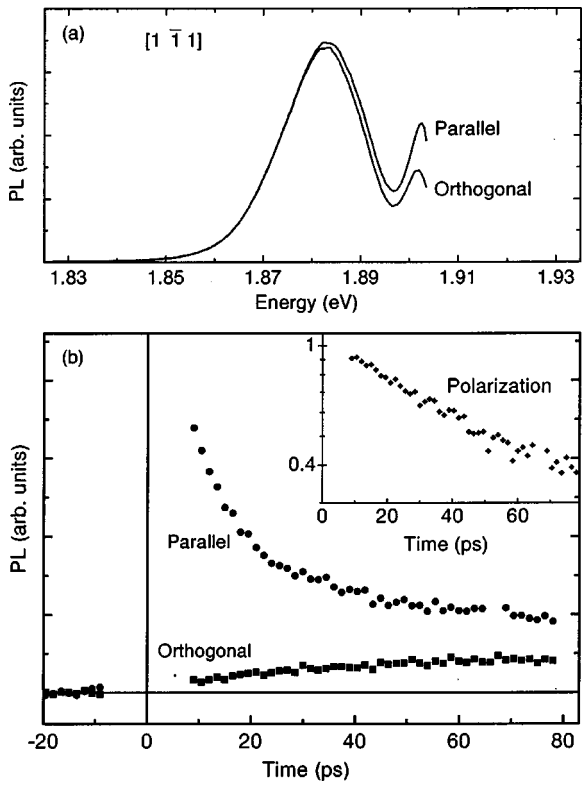

FIG. 4. Time-integrated and time-resolved PL for light propagating along the $[1\bar{1}1]$ (ordering) direction. All other conditions identical to Fig. 2.

result of the valence band splitting.[13] Therefore, the alternate assumption of an unrelaxed hole population is reasonable for ordered $Ga_xIn_{1-x}P$.

Comparison of Table I and Figs. 2 and 4 support a hole population that is largely unrelaxed, giving a $t=0$ polarization of 1 and $\frac{3}{4}$ for the ordering and growth directions. The polarization data of Fig. 2(b) actually extrapolates to a polarization *larger* than $\frac{3}{4}$ at $t=0$, which we attribute to a substrate tilt of 6°, and an excitation/collection geometry that adds another 6–7° of tilt. Our general result for unrelaxed holes, column 1 of Table I, is

$$\rho(t=0)=\frac{4\cos^2\theta}{(1+\cos^2\theta)^2}, \tag{2}$$

where θ is the angle between light and ordering. Near $\theta=55°$, this is a sensitive function of θ, and a 12° tilt pushes the value from 0.75 to 0.91, in good agreement with Fig. 2. However, near $\theta=0$, the function varies only slowly from $\rho=1$. Table I column 1 is therefore in good agreement with Figs. 2–4.

The spin-polarized PL measurements here and in Ref. 3 verify the HH nature of the 1.90-eV transition in ordered $Ga_xIn_{1-x}P$. To study spin populations in the higher-energy peaks, outside of the PL spectrum, we have used time-resolved differential absorption. In differential absorption, the absorption bleaching caused by a pump-induced spin-polarized carrier population is measured by a circularly polarized probe beam. The method has the advantage of fast time resolution,[14] multichannel detection,[15] and greater immunity to scattered laser light. A 1 micron-thick sample was

TABLE I. Computed maximum polarization, ρ, for resonant HH exciton PL in ordered $Ga_xIn_{1-x}P$ with the light k vector along the directions shown, and for the cases of hole spin completely unrelaxed, or completely randomized. Electron spin is unrelaxed from its initial state.

	Holes unrelaxed	Hole relaxed
$\mathbf{k}=[1\bar{1}1]$	1	1
$\mathbf{k}=[001]$	3/4	1/4

grown under conditions similar to those for the sample used in the previous measurement and with a HH-CB transition energy of 1.928 eV. The excitation energy was near resonance, and other experimental parameters were similar to Ref. 16.

Figure 5 shows the broadband bleaching signal (absorbance without pump-absorbance with pump) for parallel and orthogonal pump and probe beams. The 26 meV-wide σ^+ pump is tuned to the low energy side of the HH exciton in order to selectively excite from the HH valence band. The probe measures the absorption 5 ps after the excitation. In general, differential absorption spectra may result not only from state filling (bleaching), but also from broadening and shifting of the resonances as well. However, for this discussion, we concentrate on the signal centered at the HH, LH, and SO transitions, and in particular, we consider only the

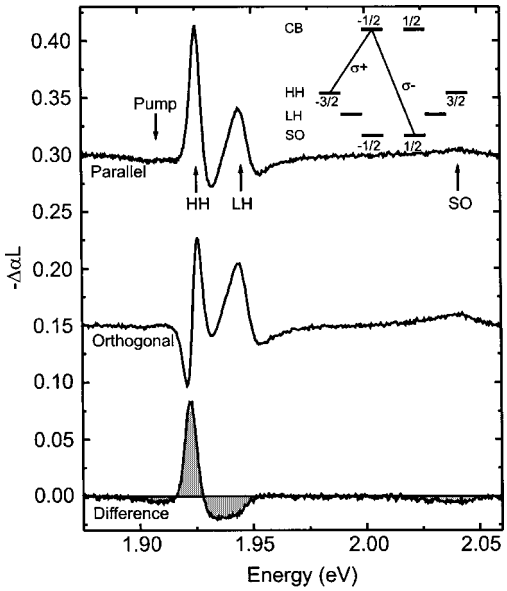

FIG. 5. Time-resolved differential absorption, $-(\alpha_{\text{pumped}}-\alpha_{\text{unpumped}})L$, where L is the sample thickness, 1 μm. The pump is 26-meV full width at half maximum, centered at 1.908 eV, 5 ps before the probe pulse, and the same energy density used in the PL measurements. Pump and probe are circularly polarized, along the [001] growth direction. Curves, top to bottom, are probe ∥ pump, probe ⊥ pump, and the computed difference, (parallel-orthogonal). The difference curve is shaded to emphasize the sign of the signal at each transition. Inset: Level diagram showing the spin-degenerate states near the bandedge for a zinc-blende semiconductor with valence-band splitting. Each state is labeled with m_j. The two transitions shown will both be blocked by a population of spin-down electrons.

sign of the polarization, i.e., $\Delta\alpha_{\text{parallel}} - \Delta\alpha_{\text{orthogonal}}$. This difference, plotted in the lower curve of Fig. 5, is positive at the HH and changes sign for the LH and SO transitions. The HH and SO anisotropies verify the spins assigned to the level diagram in Fig. 5. Resonant excitation by the σ^+ pump beam results in a population of spin-down electrons and heavy holes. Depending on their degree of spin-relaxation, both populations will block subsequent HH-CB absorption of σ^+ probe light, whereas only the electrons will block the SO-CB absorption. Because this transition begins from a $J=\frac{1}{2}$ states, the spin-down electron population will block its absorption of σ^- light, giving the sign change in Fig. 5.

The sign change at the LH energy in Fig. 5, however, is unexpected from $|\mathbf{k}|=0$ selection rules. The simple level diagram in the inset is appropriate for light propagation along the ordering axis. For light along the [001] axis, as required in a transmission measurement, the absorption peak labeled ''LH'' is actually a strong mixture of $J=\frac{3}{2}$ and $J=\frac{1}{2}$ holes. The free carrier differential absorption calculated from [001] matrix elements predicts a LH absorption anisotropy with the same sign as that of the HH, i.e., opposite Fig. 5. Calculated HH and SO anisotropies are qualitatively unchanged by the $[1\bar{1}1]\rightarrow[001]$ rotation.

In conclusion, the degree of spin-polarized PL in ordered $Ga_xIn_{1-x}P$ depends strongly on the direction of light propagation and the ordering direction. In the first few picoseconds after excitation, nearly completely polarized PL occurs along the ordering direction, and completely depolarized PL occurs orthogonal to this direction. This confirms the spin properties of the band-edge states in ordered $Ga_xIn_{1-x}P$, and eliminates the possibility of a subpicosecond hole-spin relaxation. Time-resolved absorption measurements observe the opposite spin of LH and SO transitions relative to the HH.

We would like to thank C. Kramer for the growth of the samples. This work was supported by the Office of Energy Research, Materials Science Division of the DOE under Contract No. DE-AC36-83CH10093.

[1] R. C. Miller, D. A. Kleinman, W. A. Nordland, Jr., and A. C. Gossard, Phys. Rev. B **22**, 863 (1980).
[2] Tohru Suzuki, Mater. Res. Bull. **22**, 33 (1997).
[3] T. Kita, M. Sakurai, K. Bhattacharya, K. Yamashita, T. Nishino, C. Geng, F. Scholz, and H. Schweizer, Phys. Rev. B **57**, R15 044 (1998).
[4] Hyeonsik M. Cheong, F. Alsina, A. Mascarenhas, J. F. Geisz, and J. M. Olson, Phys. Rev. B **56**, 1888 (1997).
[5] B. Fluegel, A. Mascarenhas, J. F. Geisz, and J. M. Olson, Phys. Rev. B **57**, R6787 (1998).
[6] G. S. Horner, A. Mascarenhas, R. G. Alonso, D. J. Friedman, K. Sinha, K. A. Bertness, J. G. Zhu, and J. M. Olson, Phys. Rev. B **48**, 4944 (1993).
[7] P. Ernst, C. Geng, F. Scholz, and H. Schweizer, Appl. Phys. Lett. **67**, 2347 (1995).
[8] Jagdeep Shaw, IEEE J. Quantum Electron. **24**, 276 (1988).
[9] A. M. Weiner, J. P. Heritage, and E. M. Kirschner, J. Opt. Soc. Am. B **5**, 1563 (1988).
[10] P. Ernst, C. Geng, F. Scholz, and H. Schweizer, Phys. Status Solidi B **193**, 213 (1996).
[11] *Optical Orientation*, edited by F. Meier and B. P. Zakharchenya (North-Holland, Amsterdam, 1984).
[12] R. J. Seymour and R. R. Alfano, Appl. Phys. Lett. **37**, 231 (1980).
[13] M. I. Dyakonov and V. I. Perel, in *Optical Orientation* (Ref. 11), p. 33.
[14] Atsushi Tacheuchi, Shunichi Muto, Tsuguo Inata, and Toshio Fujii, Appl. Phys. Lett. **56**, 2213 (1990).
[15] M. Joffre, D. Hulin, and A. Migus, Phys. Rev. Lett. **62**, 74 (1988).
[16] B. Fluegel, Y. Zhong, H. M. Cheong, A. Mascarenhas, J. F. Geisz, J. M. Olson, and A. Duda, Phys. Rev. B **55**, 13 647 (1997).